Chế tạo hạt nano alginate-chitosan chứa ovalbumin bằng phương pháp phun điện đồng trục để định hướng phân phối protein

TÓM TẮT

Liệu pháp protein đã phát triển vượt trội như liệu pháp hiệu quả và độc đáo vì những lợi ích to lớn của chúng trong lĩnh vực dược phẩm. Nghiên cứu này đã phát triển các hạt nano alginate-chitosan (ALG-CHI) chứa ovalbumin (OVA) bằng cách sử dụng điện phun đồng trục mà không cần tác nhân liên kết chéo để cung cấp protein OVA qua đường uống để định hướng liệu pháp protein. Các thông số tối ưu bao gồm điện áp 21 kV, lưu lượng 0,1/0,2 $mL.h^{-1}$ (lõi/vỏ), khoảng cách thu mẫu 10 cm, nồng độ polyme 4 wt% CHI và 0,5 wt% ALG. Các hạt nano ALG-OVA@CHI thu được có hình cầu, bề mặt nhẵn, không kết tụ và cấu trúc lõi-vỏ được quan sát thấy bằng hình ảnh SEM và TEM. Các hạt nano có đường kính thủy động là 313,0 ± 129,9 nm và thế zeta là +1,6 mV ở pH trung tính, được đo bằng thiết bị DLS. Đáng chú ý là các hạt nano ALG-OVA@CHI đã bao bọc OVA ở mức cao với hiệu suất 99,04 ± 0,14%, bảo vệ OVA khỏi axit dạ dày và tạo điều kiện cho OVA giải phóng kéo dài trong điều kiện đại tràng mô phỏng trong ít nhất 8 ngày. Việc giải phóng các hạt nano này chủ yếu được kiểm soát bởi sự khuếch tán của OVA và sự phân hủy polyme trong môi trường giải phóng, theo cơ chế vận chuyển không phải Fickian của Korsmeyer-Peppas. Những phát hiện này cho thấy thiết kế ALG-OVA@CHI có tiềm năng trở thành một công thức uống để cung cấp protein.

Từ khoá: *alginate, chitosan, phun điện đồng trục, hạt nano, ovalbumin*

Fabrication of ovalbumin-loaded alginate-chitosan nanoparticle using coaxial electrospray for protein delivery orientation

ABSTRACT

Protein therapeutics have emerged as effective and unique therapies because of their vast benefits in the pharmaceutical field. This study developed ovalbumin (OVA) loaded alginate-chitosan (ALG-CHI) nanoparticles using coaxial electrospray without a cross-linking agent to orally deliver OVA protein for protein therapeutics orientation. The optimal parameters include a voltage of 21 kV, a flow-rate of 0.1/0.2 $mL.h^{-1}$ (core/shell), a working distance of 10 cm, polymer concentrations of 4 wt% CHI and 0.5 wt% ALG. The obtained ALG-OVA@CHI nanoparticles had a spherical shape, smooth surface, no aggregation, and core-shell structure observed by SEM and TEM images. The nanoparticles had a hydrodynamic diameter of 313.0 ± 129.9 nm and a zeta potential of +1.6 mV at neutral pH, as measured by DLS equipment. Remarkably, the ALG-OVA@CHI nanoparticles highly encapsulated OVA with 99.04 ± 0.14% efficiency, protected it from gastric acid in the stomach, and facilitated sustained release OVA in the simulated colonic condition for at least 8 days. The release of these nanoparticles were primarily controlled by the diffusion of OVA and polymer disintegration in the release media, followed the Korsmeyer-Peppas non-Fickian transport mechanism. These findings suggested that the ALG-OVA@CHI design had potentials as an oral formulation for protein delivery.

Keywords: *alginate, chitosan, coaxial electrospray, nanoparticle, ovalbumin*

1. INTRODUCTION

Protein therapeutics have been rapidly developed in the pharmaceutical industry due to their efficacy in both diseases preventions and treatments by modulating the physiological or pathological processes of their targets.[1-2] Proteins' primary pharmacological activities in therapeutic processes include i) replacing a deficient or abnormal protein, ii) augmenting an existing pathway, iii) providing a novel function or activity, iv) interfering with a molecule or organism, and v) delivering a payload such as a radionuclide, cytotoxic drug, or protein effector.[3] Many potentially fatal diseases, including cancer, cardiovascular disease, and diabetes, have been effectively treated by proteins.[2] Moreover, proteins possess high specificity, selectivity, potency, and low toxicity, which are less likely to interfere with normal biological processes and cause adverse effects.[4-5] Furthermore, macromolecular proteins have a significantly larger surface area for molecular binding, allowing access to a much broader range of protein targets while reducing the possibility of off-target effects.[6] Protein therapeutics are most commonly administered via parenteral administrations such as injection or intravenous infusion.[1,7] The routes; however, contain several drawbacks including being expensive, painful, inconvenient, and requiring professional healthcare staff. Therefore, there has recently been a shift toward producing needle-free biopharmaceuticals such as the oral protein therapeutics.[7]

For this reason, developing effective oral formulations and increasing intact protein absorption into the intestinal mucosa is currently a major focus.[8] Furthermore, the oral route allows protein treating expression at specific locations, particularly mucosal sites, resulting in accurate and long-lasting therapy. However, direct oral protein delivery faces a number of challenges, including protein degradation in the extreme environment of the gastrointestinal tract, uncontrolled protein release, and ineffective mucosal permeability, all of which contribute to comparatively poor performance when compared to injectable administration.[9] To enhance the treatment efficacy, the proteins must be able to pass through several physicochemical and biological barriers in the digestive tract, while also providing adequate drug concentrations at the disease state. To address these

challenges, biopolymer-based nanoparticles have been used as protein delivery carriers to stabilize proteins against external obstacles and improve the bioavailability of entrapped proteins in the gastrointestinal tract.[4,10]

Alginate (ALG) is a natural polyanionic (due to carboxylic groups) biopolymer that has been prioritized as a protein carrier due to its interesting biopharmaceutical properties, such as pH sensitivity, biocompatibility, biodegradability, muco-adhesiveness, no toxicity, and no immunogenicity.[11] ALG has been extensively investigated and used in a variety of biomedical delivery systems.[12-14] However, ALG has a gel structure that is typically sensitive to chelating compounds such as phosphate, citrate, ethylenediaminetetracetic acid (EDTA), and lactate, as well as anti-gelling cations found in the gastrointestinal tract.[15] As a result, it is necessary to improve its stability by coating the ALG nanoparticles with another positively charged polymer such as chitosan (CHI).

CHI is a biopolymer with beneficial biological properties such as biocompatibility with protein antigens, good biodegradability, and low toxicity.[16-18] Moreover, CHI has excellent mucoadhesive properties due to electrostatic interactions between positively charged polymers and negatively charged mucosal surfaces, as well as advanced penetration ability across the colonic wall [19]. CHI is one of the most promising positively charged coating materials for improving the stability of encased proteins. As a result, coating ALG nanoparticles with CHI (ALG@CHI) could form a polyelectrolyte complex through ionic interaction, which was expected to reduce porosity, encapsulated protein leakage, and increase stability across wide pH ranges and enzymatic activities.[15] Furthermore, the ALG@CHI nanoparticle system has been demonstrated to exhibit synergistic effects, since the CHI infiltrate through the mucus layer and facilitates the opening of tight junctions in epithelial cells, allowing macromolecular proteins to travel paracellularly,[20] and the mucoadhesive ALG extends the time that a protein remains at adsorption sites. This ultimately improves the efficacy and bioavailability of oral protein therapies.

In this study, efforts were made to develop an oral delivery system that loaded ovalbumin (OVA), a model protein, with CHI and ALG, resulting in ALG-OVA@CHI nanoparticles. OVA has been widely utilized in protein therapeutics research due to its convenient stability at room temperature and cost effectiveness.[21] From the viewpoint of protein structure, OVA contain disulfide links in their molecular chains; as is known, the disulfide linkages have a remarkable antioxidation-reduction function.[22] The OVA-loaded polymeric nanoparticles are fabricated through the advanced coaxial electrospraying (CES) method. The CES technique is a simple one-step method for encapsulating proteins, which involves applying a high electric field to the capillary needle. The proteins and organic solvents flow through the internal capillary needle, while polymer solutions flow through the external capillary needle. The high electric charges in the liquid droplet at the needle tip result in the formation of nanoparticles via Coulomb fission.[23,24] The advantage of this method is that it is possible to prepare nanoparticles without the use of cross-linking agents. Therefore, the produced nanoparticles can robustly release the OVA protein in an appropriate environment, supplying the required dosage, allowing the therapy to take place quickly within a specific time. Furthermore, the biodegradable polymeric system can be safely removed from the body without causing harm in the long term, whereas the cross-linker might remain in the body for an extended period. Besides, compared to other nanoparticle production methods, the CES method is widely used for protein nanoparticle preparation because it reduces protein denaturation by using less solvent. This method's other advantages include ease of processing, high drug encapsulation, and a narrower range of size distribution.[25,26] As a result, CES technology is expected to produce uniform ALG-OVA@CHI nanoparticles with high encapsulation efficiency and controllable release properties in the gastrointestinal tract.

2. MATERIALS AND METHODS

2.1 Materials

OVA (78%), phosphate buffer saline (PBS, pH 7.4) were offered by Himedia, India. CHI (deacetylation of 92%) was supplied by Cemaco company, Vietnam. ALG sodium salt (low viscosity, ≤200 mPa.s) was purchased from Shanghai Zhanyun Chemical, China. Acetic acid (CH3COOH, 99.5%), sodium hydroxide (NaOH, 99%), and hydrochloric acid (HCl, 37%) were obtained from Xilong, China. All other chemicals were used without further purification.

2.2 Preparation of the material solutions

The core solutions were prepared by dissolving accurate amounts of ALG (0.05 g, 0.1 g, and 0.15 g) in 10 mL of distilled water under stirring at 60 rpm for 6 h at room temperature to get 0.5 wt%, 1 wt%, and 1.5 wt% ALG solutions, respectively. Subsequently, 0.0125 g OVA was added into the ALG solutions and stirring at 60 rpm for 3 h at room temperature to attain the homogeneous core solutions. The 4 wt% CHI shell solution was obtained by adding 0.4 g CHI into 10 mL of 90% (v/v) acetic acid under agitating at 60 rpm within 24 h at room temperature.

2.3 Fabrication of ALG-OVA@CHI nanoparticles

The ALG-OVA@CHI nanoparticles were fabricated by a single-step CES method, using equipment consisted of a high-voltage supply (GENVOLT 73030, USA), syringe pumps, a stainless steel capillary needle, 1-mL plastic syringes, and aluminum nanoparticle collector.

Briefly, the prepared core solutions (0.0125 g OVA + 0.5 wt%/1 wt%/1.5 wt% ALG) and shell solution (4 wt% CHI) were injected into syringes that connected to coaxial capillary needle. The high voltage (19, 21, and 23 kV) were applied to the capillary needle tip. The distance between the needle tip and the collector (10, 13, and 16 cm) were investigated. The core and shell solutions flow rate was at 0.1 $mL.h^{-1}$ and 0.2 $mL.h^{-1}$, respectively.[27] During the CES process, the droplets moved to collector while the solvent was allowed to evaporate and the nanoparticles were acquired at the collector. Successively, the obtained nanoparticles were dispersed in absolute ethanol to remove the free OVA.[28] Afterward, centrifugation was conducted at 10,000 rpm for 15 min at 5°C to collect the nanoparticles. The particles were then placed in petri dishes and left to undergo solvent evaporation at room temperature, resulting in the final nanoparticles product.

2.4 Characterizations of physicochemical properties

Scanning electron nanoscopy (SEM, Hitachi S-4800, Japan) and an optical nanoscope (Nikon EPIPHOT 200, Japan) was used to investigate the shape and surface morphology of two different types of nanoparticles. Samples were sputter coated with a conductive layer of platinum for SEM analysis, then scanned in a low vacuum chamber with a focused electron beam at 10 kV and magnifications of 10,000 and 60,000. As the image formed, secondary electrons emitted by the samples were detected. Transmission electron nanoscopy (TEM) was used to investigate the nanostructure of OVA@CHI and OVA@CHI@ALG particles on the JEM-1400 Flash in Jeol, Japan, at an acceleration voltage of 120 kV and magnification of 80,000 in a vacuum environment. To prepare the sample for measurement, the nanoparticle suspensions were diluted in ethanol and placed on a cellulose net.

The particle size and zeta potential of both nanoparticles were determined using the dynamic light scattering (DLS) technique in a Zetasizer on SZ-100Z2, Horiba, Japan. A 5 mL sample was prepared in alcohol and measured at a holder temperature of 25°C and a scattering angle of 90°. The results were expressed as mean ± standard deviation, with a zeta potential dimension of mV.

To investigate the chemical structures and interactions between components in nanoparticles, a Fourier transform infrared spectrometer (FTIR Nicolet 6700, Thermo Fisher Scientific, USA) was used to record FTIR spectra of samples. The scanning parameters were a wavelength range of 4000-400 cm^{-1} and a resolution of 4 cm^{-1}. The spectra samples show their characteristic peaks in the wavenumber range.

2.5 Determination of OVA encapsulation efficiency

The encapsulation efficiency of the ALG-OVA@CHI nanoparticles was assessed by dispersing 10 mg of the particles in 20 mL of distilled water and executing ultrasonic process for 280 min. Every 40 min, 2 mL of the sample was centrifuged at 10,000 rpm for 3 min at 5°C[29,30] to collect the supernatant and the nanoparticles were re-dispersed in water to continue the experiment. From the resulting supernatant, 1 mL was mixed with 2 mL of Bradford reagent and allowed to react for 3 min. The concentration of OVA was determined using UV-Vis spectroscopy method at a detection wavelength of 595 nm, which based on the standard curve equation of $y = 7.6119x + 0.7886$ ($R^2 = 0.9977$). Each determination was conducted in triplicate, the encapsulation efficiency (H%) was calculated using the formula (1), and the results were displayed in term of means ± standard deviation (SD).

$$H\% = \frac{\text{Encapsulated mass of OVA}}{\text{Total mass of OVA}} \times 100 \quad (1)$$

2.6 In vitro OVA release test

The release behavior of OVA from ALG-OVA@CHI nanoparticles was investigated in PBS solution with different pH values of 1.2 and 7.4, simulating the gastric and colonic parts of the digestive tract, respectively.[31,32] Briefly, 10 mg of the dried nanoparticle was immersed in 20 mL release medium, which were incubated at 37 ± 1°C within 8 days. At the predefined time intervals, 1 mL of sample were taken out from the release solution and centrifuged, then, it was mixed with 2 mL Bradford reagent for protein quantification at 595 nm.[29,30] To the release media, 1 mL of fresh buffer medium were returned. The amount of OVA protein released were calculated based on the calibration curve of y = 7.5107x + 0.7508 (R2 = 0.9966) for pH 1.2 and y = 8.1714x + 0.7458 (R2 = 0.9952) for pH 7.4. All measurements were performed in triplicate for reliable data and the cumulative OVA release was calculated using the following formula (2):

$$\text{Cumulative release } (\%) = \frac{C_t V_0 + v\sum_1^{t-1} C_i}{M_0 - \sum_1^{t-1} M_i} \times 100 \quad (2)$$

Where C_t, C_i were the released OVA concentrations at the time point t and i, V0 was the total volume, V was the withdrawal volume (1 mL), and M_0, M_i were the initial OVA amount and withdrawal OVA amount at the time point i.

Release kinetic models

The general mathematical models were employed to evaluate the protein release kinetics, including the zero-order (3), first-order (4), Higuchi (5) and Korsmeyer-Peppas (6) kinetic models.

Zero-order kinetic model: indicates that the rate of protein release is independent of the protein concentration in the nanoparticles. In another words, constant amount of protein is released in a time-dependent manner. Model expression:

$$M_t = M_0 + k_0 t \quad (3)$$

First-order kinetic model: describes a release rate proportional to the amount of drug remaining in the nanoparticles, or the release rate decreases as the protein concentration decreases over time. Model expression:

$$\ln M_t = \ln M_0 - k_1 t \quad (4)$$

Higuchi kinetic model: argues that the rate of drug release is related directly to the concentration gradient within the nanoparticles by expressing the drug release amount as a square root of a time-dependent process. Model expression:

$$M_t = k_H t^{\frac{1}{2}} \quad (5)$$

Korsmeyer-Peppas kinetic model: characterizes the mechanism of protein release from the polymeric nanoparticle systems, including diffusion, swelling, erosion or a complex release profile of an initial burst release followed by a sustained release. Model expression:

$$\frac{M_t}{M_0} = k_{KP} t^n \quad (6)$$

Where M_0, M_t are the initial amount of OVA and the released OVA at the time point t; whereas k_0, k_t, k_H, and k_{KP} are the release constants of the zero-order, first-order, Higuchi and Korsmeyer-Peppas models, respectively. In Korsmeyer-Peppas model, the n value is the release exponent indicative of the mechanism of transport of the protein through the polymeric matrix, in which $0 < n < 0.45$, it is Fickian diffusion, $0.45 < n < 0.89$ is non-Fickian diffusion or abnormal release, and $n > 0.9$ is skeleton dissolution mechanism.

3. RESULTS AND DISCUSSIONS

3.1 Factors affecting ALG-OVA@CHI nanoparticles formation

To find the optimal formulating condition, this study aimed to comprehend how applied voltage, ALG concentration, and injector-to-collector distance affect the morphology and size of the ALG-OVA@CHI nanoparticles. The examined parameters included voltage levels (19, 21, and 23 kV), ALG concentrations (0.5 wt%, 0.1 wt%, and 1.5 wt% w/v), and working distances (10, 13, and 16 cm).

3.1.1 Effect of the applied voltage

The effect of different voltage levels (19, 21, and 23 kV) on the SEM morphology of ALG-OVA@CS nanoparticles were firstly investigated (Figure 1). To that end, the Taylor cone plays a crucial role in the CES process as it enables the formation of uniform and stable droplets, which ultimately determine the morphology and size of the nanoparticles.

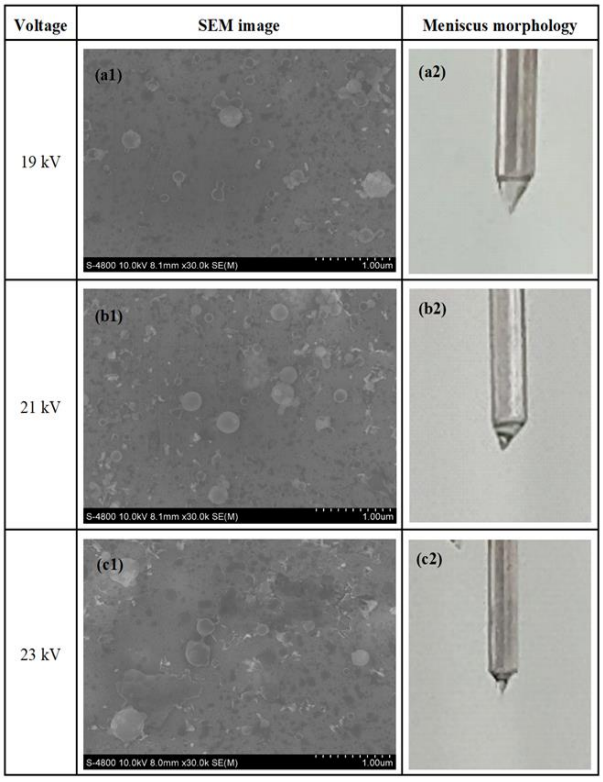

Figure 1. SEM images of ALG-OVA@CHI nanoparticles and meniscus morphology at different voltage of 19, 21, and 23 kV

At 19 kV, the prepared nanoparticles had a nearly spherical shape but possessed an uneven size distribution (Figure 1a). This was ascribed to the low imposed voltage that leads to insufficient electrical force to overcome the hydrodynamic forces, including the viscous force, the surface tension, and the frictional force.[33] The imbalance of these forces caused the formation of unstable conical meniscus at the needle tip.[34] In this case, the CES mode was considered as the nano-dripping mode, resulting in heterogeneous nanoparticles.[35] Increasing the voltage to 21 kV produced spherical nanoparticles and smooth surfaces with relative more uniform size (Figure 1b). It was attributed to the more balanced forces that formed a stable Taylor cone. In addition, the interface between the inner and outer solutions was obvious during this status, contributing to the establishment of the stable cone-jet mode. However, when the voltage was further increased to 23 kV, the nanoparticles had rough surfaces and did not achieve a fully spherical shape (Figure 1c). It was explained that the surface tension was substantially reduced while the electric field dominated the hydrodynamic force, resulting in the stretching of meniscus tip. Furthermore, the interface was vibratile and difficult to observe, suggesting that the pulsed cone-jet regime was created at 23 kV. As a result, the findings indicated that a voltage of 21 kV was ideal for obtaining ALG-OVA@CHI nanoparticles with desired properties.

3.1.2 Effect of the ALG concentration

ALG concentration plays an important role in the protection and sustained release of proteins by polyelectrolyte complexation with CHI. The nanoparticles produced at an ALG concentration of 0.5 wt% had a spherical shape along with secondary droplets appearance (Figure 2a), which proved that the Taylor cone was successfully created at this concentration. However, undesirable results attained when the ALG concentrations increased to 1 wt% and 1.5 wt% (Figure 2b, 2c), which yielded sparse-and-undeveloped nanoparticles.

Table 1. Mean diameter and PDI value of ALG-OVA@CHI nanoparticles at different ALG concentrations with the fixed voltage of 21 kV and solution flow rate of 0.1/0.2 mL/h (core/shell)

ALG concentration (wt%)	Mean diameter (nm)	PDI
0.5	313.0 ± 129.9	0.202
1	393.5 ± 172.7	0.395
1.5	398.3 ± 195.1	0.022

At higher ALG concentrations, the solution become more viscous, and the higher viscosity leads to the requirement of more energy to spray the polymer solution from the meniscus.[36] Therefore, while the imposed energy was kept constant, it was inefficiently to transform the liquid into nanoparticles. Additionally, as the ALG concentrations increased, the gravity of polymer solution boosted up abundantly, thereby the meniscus tended to be elongated, as in the case of ALG 1.5 wt%. Moreover, the nanoparticle sizes were also increased from ~300 nm to ~400 nm, with increasing ALG concentrations (Table 1). Furthermore, all PDI values exhibit regular particle size distributions (PDI < 0.3). Conclusively, to produce particles of a minimum size range with narrow size distribution, the ALG concentration of 0.5 wt% was selected for future experiments.

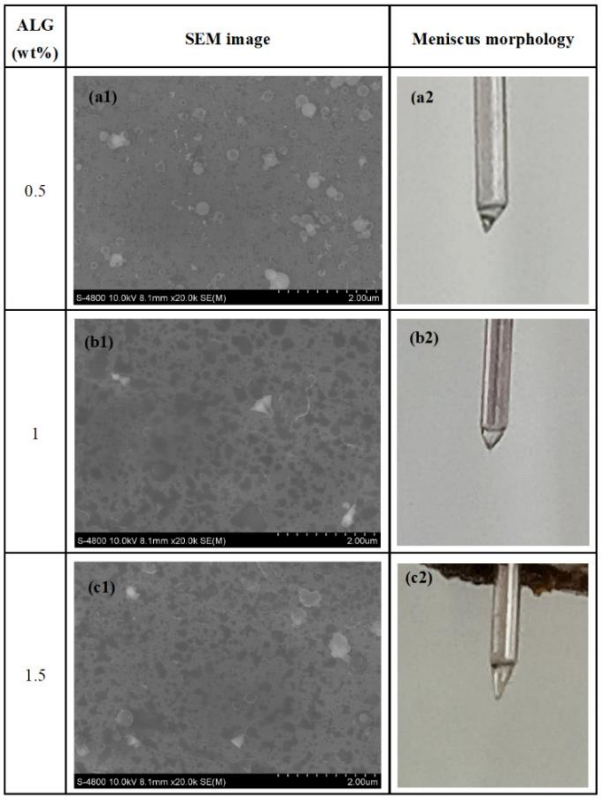

Figure 2. SEM images of ALG-OVA@CHI nanoparticles and meniscus morphology at different ALG concentration of 0.5%, 1%, and 1.5%

3.1.3 Effect of the needle tip-to-collector distance

Besides the applied voltage and the material concentration, the needle tip-to-collector distance is another factor that plays a significant role in the performance and stability of the granulation process.[31,37] Figure 3 demonstrates nanoparticles produced at various distance of 10, 13, and 16 cm.

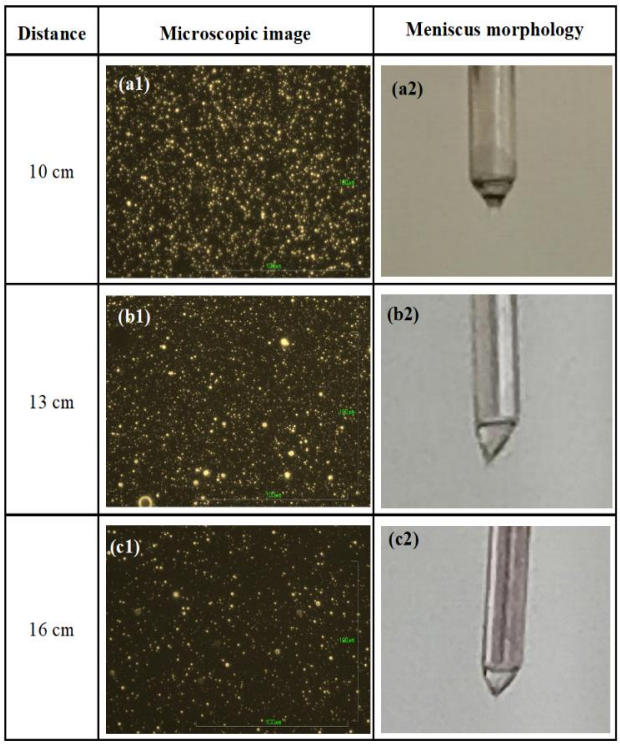

Figure 3. Nanoscope images of ALG-OVA@CHI nanoparticles and meniscus morphology at different needle tip-to-collector distances of 10, 13, and 16 cm

When the distance was set at 10 cm, the nanoparticles acquired spherical morphology and non-aggregation property, which confirmed that this distance was adequate to accomplish complete evaporation of the solvent before reaching the collector (Figure 3a). At this distance, the Taylor cone could be kept steady, forming a steady jet generated at the tip of the cone. The distance increment to 13 cm and 16 cm has two significant effects on the CES process. Firstly, the expansion in distance caused a reduction in collected nanoparticle, as they dispersed into the surrounding environment instead of depositing in the grounded collector plate to form nanoparticles, resulting in a low electrospraying performance (Figure 3b, 3c). Secondly, the conical meniscus had an unconventional morphology that was attributed to the decreased electric field strength due to a distance increase between the electrodes (the electrical field strength is defined as the applied voltage divided by the distance between the tip and collector).[34] Therefore, it was convinced that increasing the distance between the injector and the collector had a direct impact on the nanoparticle collection efficiency and the stability of the Taylor cone. In summary, the optimal needle tip-to-collector distance was set at 10 cm.

3.2 Diameter, zeta potential and structure of ALG-OVA@CHI nanoparticles

Utilizing the optimal parameter of the applied voltage of 21 kV, the flow rate of 0.1/0.2 mL.h^{-1} (core/shell), the needle tip-to-collector distance of 10 cm, and the polymer concentrations of 4 wt% CHI and 0.5 wt% ALG, the final ALG-OVA@CHI nanoparticles were further investigated their physicochemical properties.

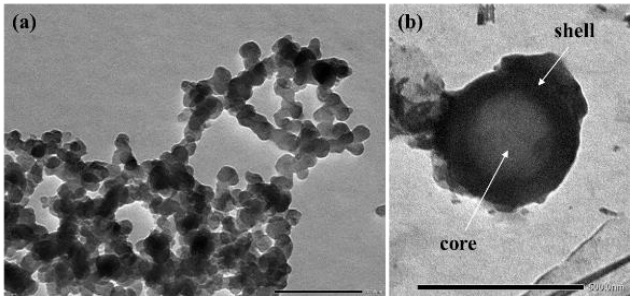

Figure 4. TEM image of (a) ALG-OVA@CHI nanoparticles and (b) the core-shell structure of the nanoparticles

The interaction of orally administered nanoparticles with the mucous epithelium in the intestinal environment is critical for protein delivery. To ensure mucosal adhesion and penetration through mucous membranes of ALG-OVA@CHI nanoparticles, the diameter and zeta potential of nanoparticles synthesized under optimal conditions were determined using the DLS technique. For this, the synthesized nanoparticles had a diameter of 313.0 ± 129.91 nm, which was appropriate diameter for mucus layer permeation (less than 500 nm).[38] Moreover, the particles possessed a zeta potential of +1.6 mV at pH 7.0, possibly due to the presence of a polycation CHI layer coating on the surface of the nanoparticles. This positively charged property allows for electrostatic interactions with the negatively charged mucus on the mucosal wall, which helps nanoparticles adhering to the mucosal surface and avoiding mucosal clearance.[39,40] Additionally, the polydispersity index (PDI) of the nanoparticles was 0.202, indicating good monodispersity in size, which contributed to the nanoparticles' large specific surface area, resulting in stable release of OVA protein, discussed in the next section. Furthermore, the TEM results showed a homogeneous size distribution and morphology (Figure 4a), with a complete core-shell structure (Figure 4b). The outer dark shell corresponds to the CHI coating, which surrounds the darkish ALG core containing uniformly distributed OVA. This demonstrated the successful fabrication of a core-shell ALG-OVA@CHI nanoparticle structure with the single-step CES technique.

3.3 Chemical characteristics

The FTIR analysis revealed important insights about the chemical characteristics and the interactions between the components in the ALG-OVA@CHI nanoparticles (Figure 5). The FTIR spectra of CHI displayed feature peaks at 3453 cm^{-1}, 1624 cm^{-1}, 1416 cm^{-1}, 1339 cm^{-1}, and 1028 cm^{-1}, corresponding to the overlapping areas of the O–H and N–H stretching vibrations, C–H stretching, N–H bending (amide I, II), C–N stretching (amide III) and C–O–C bond, respectively.[41] In the ALG spectrum, characteristic peaks at 3479 cm^{-1}, 2840 cm^{-1}, 1633 cm^{-1}, 1358 cm^{-1}, and 1045 cm^{-1} represented the –OH group stretching vibrations, C–H stretching, anti-symmetric, symmetric stretching of carbonyl groups, and C–O–C linkage, respectively.[42] Notably, in the ALG@CHI nanoparticles, the amide group of the cationic polymer (ALG) interacts with the carbonyl group of anionic polymer (ALG), resulting in the polyelectrolyte complex.[43] As a result of the interactions, the displacement of these groups were observed with a shift from 1624 cm^{-1} to 1627 cm^{-1} (amide groups) and from 1358 cm^{-1} to 1397 cm^{-1} (carbonyl groups). Additionally, the absorption at 1045–1084 cm^{-1}, relating to the elongation of C–O–C bonds, confirmed the effective interactions between CHI and ALG in their structure.

In the ALG-OVA@CHI nanoparticle spectrum, a broader and intense band centered at 3468 cm^{-1} corresponded to stretching vibrations from the overlapping areas of the O–H bond in the polymer structures and N–H of amide group in the protein structures. The peaks observed at 2921 and 2855 cm^{-1} were due to symmetric and asymmetric C–H stretching vibrations of pyranose ring.[44] Characteristic bands of CHI, ALG, and OVA were usually seen in the range 1600–1650 cm^{-1}, correlated with N–H bending (amide I), C–O stretching (carbonyl group) and C–O stretching (amide I), repestively. Those bands shifted and overlapped each other, creating a strong peak at 1609 cm^{-1}. The dissappearance of the symmetric carbonyl group (signal at 1397 cm^{-1}), in comparation to ALG@CHI spectrum, comfirmed the completely encapsulation of ALG within CHI nanopaticle. The elongation of C–O–C linkage was shifted in the ALG-OVA@CHI nanoparticle, from 1084 cm^{-1} to 1095 cm^{-1}, which reveals the

successfully encapsulation of OVA protein in the nanoparticle. This result is also consistent with previous study by Cao et al. (2024).[45]

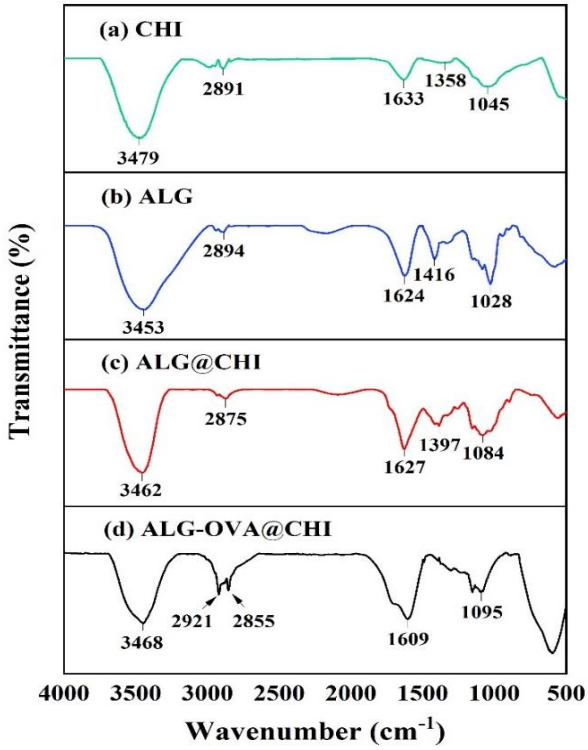

Figure 5. FTIR spectra of (a) CHI, (b) ALG, (c) ALG@CHI nanoparticle and (d) ALG-OVA@CHI nanoparticle

3.4 Encapsulation efficiency

The encapsulation efficiency of ALG-OVA@CHI was determined using UV-Vis measurement as it directly measures the OVA protein entrapment. In this experiment, distillated water was used as medium to disperse the nanoparticles, which could dissolve OVA completely and had no interference between protein and Bradford reagent. The OVA encapsulation efficiency of the nanoparticles was 99.04 ± 0.14% (Figure 6), which was significantly higher than those in other reports.[32,46] This result indicated that the CES technique is an effective method to fabricate core-shell nanoparticles with outstanding encapsulation efficiency. The reasons for this is that the nanoparticles preparation process happened in the air phase, not the liquid phase, thus limiting the diffusion and loss of OVA. In addition, as previously discussed, the CES technique could provide highly dispersed and distributed OVA within CHI and ALG polymer matrix, leading to a high encapsulation efficiency. Interestingly, the formation of polyelectrolyte complex between CHI and ALG in the shell of the nanoparticles were considered as a self-assembly cross-linking process, contributing to the prevention of OVA leakage. The similar results were observed in the previous studies of Manosree et al. (2020) and Zaeim et al. (2017).[47,48]

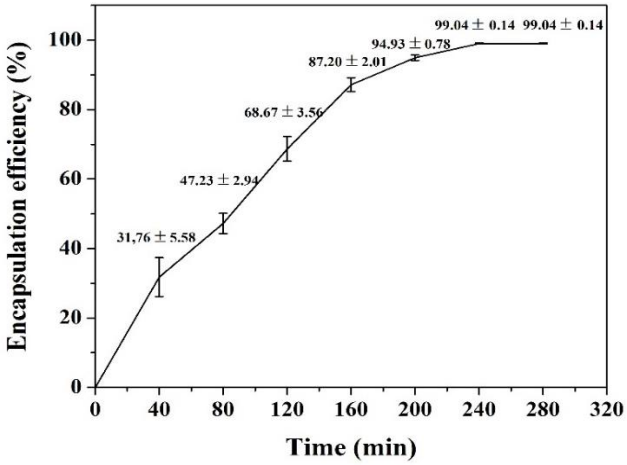

Figure 6. OVA encapsulation efficiency of ALG-OVA@CHI nanoparticles

3.5 In vitro OVA release results

In this study, OVA protein was encapsulated within ALG-OVA@CHI nanoparticles, which were expected to both protect the drug from degradation in an acidic gastric environment (pH 1.2) and exhibit sustained OVA release in a colonic environment (pH 7.4). Furthermore, the ALG-OVA@CHI design aims to improve the nanoparticles' colon-targeting characteristics by using of polycationic CHI coating. Therefore, the in vitro protein cumulative release behaviors of ALG-OVA@CHI nanoparticles were investigated in physiological medium PBS (pH 1.2 and pH 7.4) at 37^{o}C for 8 days (Figure 7).

During the first initial 2 h (i.e., the expected retention time of the nanoparticles in the gastric environment), as expected, the nanoparticles effectively retained OVA release in both the gastric (pH 1.2) and colonic (pH 7.4) conditions by limiting protein delivery to less than 30% (Figure 7a). The complexation of CHI and ALG at pH 1.2 reduced the burst release behavior of the nanoparticles. This reduction was achieved by a decrease in vacant spaces in the polymer network, which reduced the swelling of the nanoparticles, hence limiting protein burst release.[49] In detail, the protein highly released within the first 0.5 h (25.53% for pH 1.2 and 12.02% for pH 7.4), followed by a stable release until 2 h, reaching 27.51% for pH 1.2 and 19.37% for pH 7.4. This was

attributed to the free OVA's poor attachment to the nanoparticles' outermost layer/surface, resulting in rapid release. On the other hand, the encapsulated protein was released over an extended period of time, resulting in a steady release pattern for OVA. At pH 7.4, the CHI outer shell was insoluble, resulting in a dense structure. As a result, the diffusion velocity of protein out of the carrier decreased, and OVA content release in pH 7.4 was lower than that in pH 1.2. Conclusively, the ALG-OVA@CHI design could retain the drug release and avoid the drug degradation in an acidic environment, thereby meeting the study's objective.

The OVA protein release experiment was extended to 8 days to investigate the long-term release behavior and predict structural variation (Figure 7b). To this purpose, the OVA was steadily released in both pH settings, reaching maximum values of 91.41% for pH 1.2 and 93.42% for pH 7.4 after 6 days. The gradual increase in OVA release content was attributed to the structural variation of nanoparticles that had been immersed in the release medium for an extended period of time. In the acidic condition, the solubility of the CHI layer increased significantly, causing the CHI shell to dissolve faster, resulting in strong nanoparticle degradation. As a consequently, the interaction between CHI and ALG was weakened and the repulsion between molecular chains of the polymer matrix increased, thus, the ALG@CHI carrier structure could not effectively prevent OVA diffusion into the release environment.[50] Conversely, in a light alkaline environment of pH 7.4, the hydrophilicity of the carriers increased due to interactions between hydrophilic groups in polymer structure and water molecules, causing water to potentially permeate into the nanoparticles and dissolved OVA, resulting in an increase in the percentage of cumulative release. It was also worth noting that the protein content remaining after the experiments could be the result of drug interactions with carriers. The above arguments implied that the release mechanism of ALG-OVA@CHI nanoparticles produced by CES method was primarily based on the dissolution, erosion, or degradation of ALG@CHI nanocarriers at various pH values. In summary, the ALG-OVA@CHI design was identified as a potential material capable of inhibiting OVA release in gastric acidic conditions, exhibiting sustained protein release in the colonic environment, and increasing OVA bioavailability in the gastrointestinal tract, all of which contributed to the development of controlled release and orally therapeutic effectiveness.

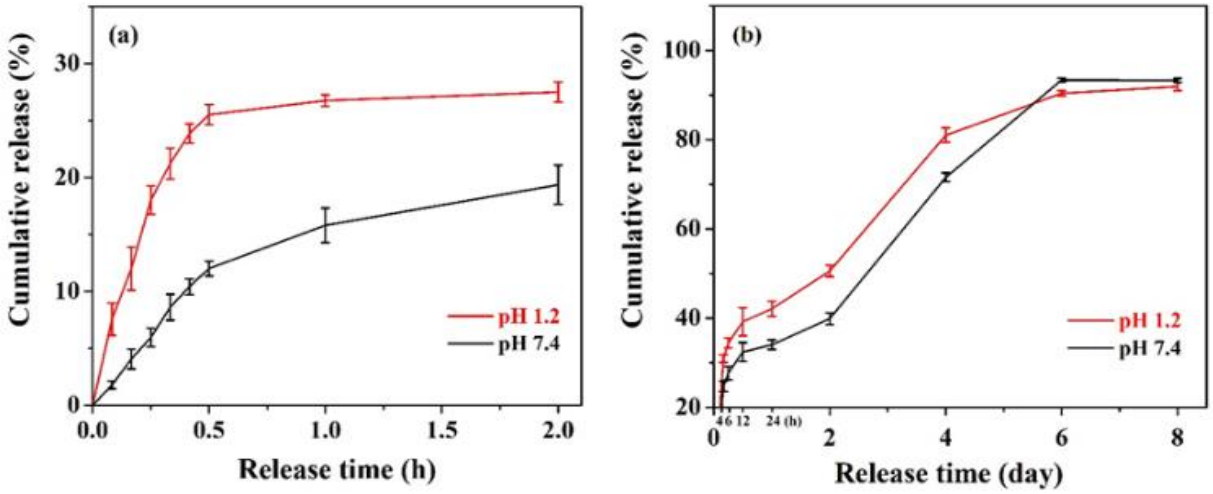

Figure 7. In vitro release profile of OVA (a) in initial 2 hours and (b) in 8 days.

Table 2. The kinetic models for the OVA release at different pH of 1.2 and 7.4 within 2 hours and 8 days

		Zero-order		First-order		Higuchi		Korsmeyer-Peppas		
		R^2	k_0	R^2	k_1	R^2	k_H	R^2	k_{KP}	n
pH 1.2	**2 h**	0.4706	10.541	0.4969	0.1278	0.7622	20.499	**0.7866**	23.150	0.4078
	8 day	0.8629	0.4288	**0.9683**	0.0132	0.9521	5.9453	**0.9772**	20.482	0.7498
pH 7.4	**2 h**	0.8077	9.2479	0.8306	0.1040	0.9103	4.4663	**0.9141**	11.918	0.3962
	8 day	0.9006	0.4777	**0.9512**	0.0143	0.9211	10.831	**0.9791**	11.634	0.4774

To better understand the releasing process of OVA, the release kinetic models were studied by fitting the release data of OVA in physiological medium PBS (pH 1.2 and pH 7.4) using zero-order, first order, Higuchi and Korsmeyer-Peppas models, and the release mechanism was obtained by the kinetic parameters that characterized the models. According to the Table 2, the Korsmeyer-Peppas kinetic model had reasonably high correlation coefficient (R^2), which was considered to be consistent with the release mechanism in all stages. The release of OVA nanoparticles under simulated gastric condition exhibited higher release rates than those at simulated colonic environment (k_{KP} at pH 1.2 > k_{KP} at pH 7.4) demonstrating that the release of OVA from CHI@ALG nanoparticles was more promoted in an acidic medium, and this assumption was compatible with the experiment as discussed in previous section. During the first phase (2 hours), the diffusion exponent (n) of the Korsmeyer-Peppas model was less than 0.45, indicating that Fickian diffusion was primarily controlling OVA release from the ALG-OVA@CHI nanoparticles. While in the entire release process (8 hours), the R^2 coefficient was better fitted with the Korsmeyer-Peppas model, and the n value was in the range of 0.45-0.89 suggesting that the OVA release followed an anomalous (non-Fickian) transport mechanism, which involved a combination of diffusion of OVA and disintegration of polymer matrix.[51] Besides, when calculating first-order release kinetics, the whole release process had a high R^2 value, contributing the decrease of release rates as the OVA concentration decreased over time corresponding to the late state of release profiles. In conclusion, the delivery system's flexibility in different phases of the release process made the ALG-OVA@CHI nanoparticles as an ideal and versatile formulation for orally protein delivery applications.

4. CONCLUSIONS

This study effectively produced an ALG-CHI nanoparticle encapsulating OVA, a model protein utilized in protein therapeutics research, utilizing the CES approach for possible protein therapies. The optimal CES parameters included an applied voltage of 21 kV, a flow rate of 0.1/0.2 $mL.h^{-1}$ (core/shell), a needle tip-to-collector distance of 10 cm, and polymer concentrations of 4 wt% CHI and 0.5 wt% ALG. The SEM and TEM images revealed that the ALG-OVA@CHI nanoparticles had a spherical shape, smooth surface, no aggregation, and a core-shell structure. The DLS measurements showed that the nanoparticles had a hydrodynamic diameter of 313.0 ± 129.9 nm and a zeta potential of +1.6 mV at neutral pH. The FTIR analysis confirmed the interactions between the nanoparticle components, such as the formation of a polyelectrolyte complex between CHI and ALG, as well as the presence of OVA in the formulation. A notable feature of the ALG-OVA@CHI nanoparticle was its encapsulation efficiency OVA reached 99.04 ± 0.14%. Under simulated gastrointestinal conditions, the ALG-OVA@CHI formulation effectively shielded the encased protein from the acidic environment of the gastric fluid, while under simulated environment, the nanoparticle demonstrated a sustained release achieving release capacity of above 90%. Additionally, the OVA protein release profiles from ALG-CHI nanoparticle primary relied in the diffusion of OVA and the dissolution of polymer network, adhering to the Korsmeyer-Peppas kinetics model. In conclusion, the nanostructure of ALG-CHI could be an excellent candidate for oral OVA delivery, contributing to the advancement of protein therapeutics.

REFERENCES

1. F. Fitriagustiani, A. Z. Mustopa, S. Budiarti, M. F. Warsito, R. D. Pratiwi, D. F. Agustiyanti, M. Nurfatwa. Formulation and Characterization of Alginate Coated Chitosan Nanoparticles as Therapeutic Protein for Oral Delivery System, *Trends in Sciences*, **2022**, 19(18), 5797-5797.
2. S. J. Cao, S. Xu, H. M. Wang, Y. Ling, J. Dong, R. Xia, X. Sun. Nanoparticles: oral delivery for protein and peptide drugs, *American Association of Pharmaceutical Scientists*, **2019**, 20(190), 1-11.
3. P. J. Carter. Introduction to current and future protein therapeutics: a protein engineering perspective, *Experimental cell research*, **2011**, 317(9), 1261-1269.
4. R. Vaishya, V. Khurana, S. Patel, A. K. Mitra. Long-term delivery of protein therapeutics, *Expert opinion on drug delivery*, **2015**, 12(3), 415-440.
5. B. Leader, Q. J. Baca, D. E. Golan. Protein therapeutics: a summary and pharmacological classification, *Nature reviews Drug discovery*, **2008**, 7, 21-39.

6. J. R. Kintzing, M. V. F. Interrante, J. R. Cochran. Emerging strategies for developing next-generation protein therapeutics for cancer treatment, *Trends in pharmacological sciences*, **2016**, 37(12), 993-1008.

7. Z. Antosova, M. Mackova, V. Kral, T. Macek. Therapeutic application of peptides and proteins: parenteral forever?, *Trends in biotechnology*, **2009**, 27(11), 628-635.

8. J. E. V. Ramirez, L. A. Sharpe, N. A. Peppas. Current state and challenges in developing oral vaccines, *Advanced drug delivery reviews*, **2017**, 114, 116-131.

9. V. Truong-Le, P. M. Lovalenti, A. M. Abdul-Fattah. Stabilization challenges and formulation strategies associated with oral biologic drug delivery systems, *Advanced drug delivery reviews*, **2015**, 93, 95-108.

10. F. M. Almutairi. Biopolymer Nanoparticles: A Review of Prospects for Application as Carrier for Therapeutics and Diagnostics, *International Journal of Pharmaceutical Research & Allied Sciences*, **2019**, 8(1), 25-35.

11. P. Severino, C. F. Silva, L. N. Andrade, D. L. Oliveira, J. Campos, E. B. Souto. Alginate nanoparticles for drug delivery and targeting, *Current pharmaceutical design*, **2019**, 25(11), 1312-1334.

12. C. Zhang, G. Shi, J. Zhang. Targeted antigen delivery to dendritic cell via functionalized alginate nanoparticles for cancer immunotherapy, *Journal of Controlled Release*, **2017**, 256, 170-181.

13. S. Mallakpour, E. Azadi, C. M. Hussain. Chitosan, alginate, hyaluronic acid, gums, and β-glucan as potent adjuvants and vaccine delivery systems for viral threats including SARS-CoV-2: A review, *International Journal of Biological Macromolecules*, **2021**, 182, 1931-1940.

14. D. Thomas, K. KurienThomas, M. S. Latha. Preparation and evaluation of alginate nanoparticles prepared by green method for drug delivery applications, *International Journal of Biological Macromolecules*, **2020**, 154, 888-895.

15. H. Liu, M. Xie, S. Nie. Recent trends and applications of polysaccharides for microencapsulation of probiotics, *Food frontiers*, **2020**, 1(1), 45-59.

16. P. Jana, M. Shyam, S. Singh, V. Jayaprakash, A. Dev. Biodegradable polymers in drug delivery and oral vaccination, *European Polymer Journal*, **2021**, 142, 110155.

17. M. Song, L. Li, Y. Zhang, K. Chen, H. Wang, R. Gong. Carboxymethyl-β-cyclodextrin grafted chitosan nanoparticles as oral delivery carrier of protein drugs, *Reactive and Functional Polymers*, **2017**, 117, 10-15.

18. A. Sogias, A. C. Williams, V. V. Khutoryanskiy. Why is chitosan mucoadhesive?, Biomacromolecules. 2008, 9(7), 1837-1842.

19. M. Kurakula, S. Gorityala, K. Moharir. Recent trends in design and evaluation of chitosan-based colon targeted drug delivery systems: Update 2020, *Journal of Drug Delivery Science and Technology*, **2021**, 64, 102579.

20. K. Sonaje, K. J. Lin, M. T. Tseng, S. P. Wey, F. Y. Su, E. Y. Chuang, C. W. Hsu, C. T. Chen, H. W. Sung. Effects of chitosan-nanoparticle-mediated tight junction opening on the oral absorption of endotoxins, *Biomaterials.* **2011**, 32(33), 8712-8721.

21. M. K. Amin, J. S. Boateng. Enhancing Stability and Mucoadhesive Properties of Chitosan Nanoparticles by Surface Modification with Sodium Alginate and Polyethylene Glycol for Potential Oral Mucosa Vaccine Delivery, *Marine Drugs.* **2022**, 20(3), 156.

22. L. Tang, Y. H. Chen, Q. Wang, X.-H. Wang, Q.-X. Wu, Z.-F. Ding. Microencapsulation of functional ovalbumin and bovine serum albumin with polylysine-alginate complex for sustained protein vehicle's development, *Food Chemistry.* **2022**, 368, 130902.

23. N. Bock, T. R. Dargaville, M. A. Woodruff. Electrospraying of polymers with therapeutic molecules: State of the art, *Progress in polymer science*, **2012**, 37(11), 1510-1551.

24. H. Xu, J. Wang, B. Li, K. Yu, J. Tian, D. Wang, W. Zhang. Effect of spray modes on electrospray cooling heat transfer of ethanol, *Applied Thermal Engineering*, **2021**, 189, 116757.

25. H. T. T. Nguyen, T. N. Tran, A. C. Ha, P. D. Huynh. Impact of deacetylation degree on properties of chitosan for formation of electrosprayed nanoparticles, *Journal of Nanotechnology*, **2022**, 2288892.

26. L. Zhang, J. Huang, T. Si, R. X. Xu. Coaxial electrospray of microparticles and nanoparticles for biomedical applications, *Expert review of medical devices*, **2012**, 9(6), 595-612.

27. Z. Mai, J. Chen, T. He, Y. Hu, X. Dong, H. Zhang, W. Huang, F. Ko, W. Zhou. Electrospray biodegradable microcapsules loaded with curcumin for drug delivery systems with high bioactivity, *RSC Advances*, **2017**, 7(3), 1724-1734 .

28. C. H. Zheng, W. Q. Liang, F. Li, Y. P. Zhang, W. J. Fang. Optimization and characterization of chitosan-coated alginate microcapsules containing albumin, *Die Pharmazie-An International Journal of Pharmaceutical Sciences*, **2005**, 60(6), 434-438.

29. N. J. Kruger. The Bradford method for protein quantitation. In: Walker JM, editors. The protein protocols handbook, *Springer Protocols Handbooks. Humana Press, Totowa*. **2009**, 17-24.

30. B. W. Lee, J. H. Ha, H.G. Shin, S. H. Jeong, J. H. Kim, J. Lee, J. Y. Park, H. J. Kwon, K. Jung, W. S. Lee. Lindera obtusiloba attenuates oxidative stress and airway inflammation in a murine model of ovalbumin-challenged asthma, *Antioxidants.* **2020**, 9(7), 563.

31. L. Zhang, J. Huang, T. Si, R. X. Xu. Coaxial electrospray of microparticles and nanoparticles for biomedical applications, *Expert review of medical devices*, **2012**, 9(6), 595-612.

32. P. Mukhopadhyay, S. Chakraborty, S. Bhattacharya, R. Mishra, P. P. Kundu. pH-sensitive chitosan/alginate core-shell nanoparticles for efficient and safe oral insulin delivery, *International journal of biological macromolecules*, **2015**, 72, 640-648.

33. X. Chen, L. Jia, X. Yin, J. Cheng, J. Lu. Spraying modes in coaxial jet electrospray with outer driving liquid. *Physics of fluids*, **2005**, 17(3), 032101.

34. J. F. Hu, S. F. Li, G. R. Nair, W. T. Wu. Predicting chitosan particle size produced by electrohydrodynamic atomization, *Chemical engineering science*, **2012**, 82, 159-165.

35. A. Sosnik. Production of drug-loaded polymeric nanoparticles by electrospraying technology, *Journal of biomedical nanotechnology*, **2014**, 10(9), 2200-2217.

36. S. Ghayempour, S. M. Mortazavi. Fabrication of micro–nanocapsules by a new electrospraying method using coaxial jets and examination of effective parameters on their production, *Journal of Electrostatics*, **2013**, 71(4), 717-727.

37. C. Chen, W. Liu, P. Jiang, T. Hong. Coaxial electrohydrodynamic atomization for the production of drug-loaded micro/nanoparticles, *Micromachines*, **2019**, 10(2), 125.

38. P. Cao, F. Y. Han, L. Grøndahl, Z. P. Xu, L. Li. Enhanced oral vaccine efficacy of polysaccharide-coated calcium phosphate nanoparticles, *ACS omega*, **2020**, 5(29), 18185-18197.

39. M. C. Gómez-Guillén, M. P. Montero. Enhancement of oral bioavailability of natural compounds and probiotics by mucoadhesive tailored biopolymer-based nanoparticles: a review, *Food Hydrocolloids*, **2021**, 118, 106772.

40. J. S. Crater, R. L Carrier. Barrier properties of gastrointestinal mucus to nanoparticle transport, *Macromolecular bioscience*, **2010**, 10(12), 1473-1483.

41. P. I Soares, A. I. Sousa, J. C. Silva, I. M. Ferreira, C. M. Novo, J. P. Borges. Chitosan-based nanoparticles as drug delivery systems for doxorubicin: Optimization and modelling, *Carbohydrate polymers*, **2016**, 147, 304-312.

42. P. Kunjumon, G. Viswanathan, S. Baby. Biocompatible madecassoside encapsulated alginate chitosan nanoparticles, their anti-proliferative activity on C6 glioma cells, *Carbohydrate Polymer Technologies and Applications*, **2021**, 2, 100106.

43. B. Sarmento, D. Ferreira, F. Veiga, A. Ribeiro. Characterization of insulin-loaded alginate nanoparticles produced by ionotropic pre-gelation through DSC and FTIR studies, *Carbohydrate polymers*, **2006**, 66(1), 1-7.

44. D. Kulig, A. Zimoch-Korzycka, A. Jarmoluk, K. Marycz. Study on alginate–chitosan complex formed with different polymers ratio, *Polymers*, **2016**, 8(5), 167.

45. L. N. H. Cao, T. V. Nguyen, N. Q. Nguyen, T. B. T. Nguyen, H. V. T. Luong, D. T. Pham. Alginate functionalized chitosan nanoparticles using multilayer co-axial electro-spraying for ovalbumin controlled release via oral delivery, *Journal of Drug Delivery Science and Technology*, **2024**, 96, 105733.

46. C. Y. Karakas, H. R. Ordu, F. Bozkurt, A. Karadag. Electrosprayed chitosan-coated alginate–pectin beads as potential system for colon-targeted delivery of ellagic acid, *Journal of the Science of Food and Agriculture*, **2022**, 102(3), 965-975.

47. M. Chatterjee, N. Jaiswal, A. Hens, N. Mahata, N. Chanda. Development of 6-thioguanine conjugated PLGA nanoparticles through thioester bond formation: benefits of electrospray mediated drug encapsulation and sustained release in cancer therapeutic applications, *Materials Science and Engineering: C*, **2020**, 114, 111029.

48. D. Zaeim, M. Sarabi-Jamab, B. Ghorani, R. Kadkhodaee, R. H. Tromp. Electrospray assisted fabrication of hydrogel microcapsules by single-and double-stage procedures for encapsulation of probiotics, *Food and Bioproducts Processing*, **2017**, 102, 250-259.

49. J. M. Unagolla, A. C. Jayasuriya. Drug transport mechanisms and in vitro release kinetics of vancomycin encapsulated chitosan-alginate polyelectrolyte microparticles as a controlled drug delivery system, *European Journal of Pharmaceutical Sciences*, **2018**, 114, 199-209.

50. X. Sun, C. Liu, A. M. Omer, L. Y. Yang, X. K. Ouyang. Dual-layered pH-sensitive alginate/chitosan/kappa-carrageenan microbeads for colon-targeted release of 5-fluorouracil, *International journal of biological macromolecules*, **2019**, 132, 487-494.

51. M. Ge, Y. Li, C. Zhu, G. Liang, J. Alam, G. Hu, Y. Gui, J. Rashid. Preparation of organic-modified magadiite–magnetic nanocomposite particles as an effective nanohybrid drug carrier material for cancer treatment and its properties of sustained release mechanism by Korsmeyer–Peppas kinetic model, *Journal of Materials Science*, **2021**, 56(25), 14270-14286.